Superconductivity of the hydrogen-rich metal hydride Li_5MoH_{11} under high pressure

Dezhong Meng,[1,*] Masafumi Sakata,[1] Katsuya Shimizu,[1] Yuki Iijima,[2] Hiroyuki Saitoh,[3] Toyoto Sato,[2] Shigeyuki Takagi,[2] and Shin-ichi Orimo[2,4]

[1]*KYOKUGEN, Graduate School of Engineering Science, Osaka University, 1–3 Machikaneyama, Toyonaka, Osaka 560–8531, Japan*
[2]*Institute for Materials Research, Tohoku University, 2-1-1 Katahira, Aoba-ku, Sendai, Miyagi 980–8577, Japan*
[3]*Quantum Beam Science Research Directorate, National Institutes for Quantum and Radiological Science and Technology, 1-1-1 Kouto, Sayo-cho, Sayo-gun, Hyogo 679–5148, Japan*
[4]*WPI Advanced Institute for Materials Research, Tohoku University, 2-1-1 Katahira, Aoba-ku, Sendai, Miyagi 980–8577, Japan*

(Received 7 September 2018; revised manuscript received 20 November 2018; published 15 January 2019)

Ternary metal hydrides are convenient and valuable systems for investigating the metallization and superconductivity of metal hydrides because they can be synthesized under mild conditions and recovered under ambient pressure. In this study, the conducting behavior and structural phase transition of a hydrogen-rich metal hydride, Li_5MoH_{11}, were investigated at pressures up to 210 GPa in a diamond anvil cell. The results showed that Li_5MoH_{11} transforms from an insulator to a poor metal at around 100 GPa. Superconductivity was observed at 100 GPa and retained until 210 GPa, and its maximum onset transition temperature was 6.5 K at 160 GPa. High-pressure synchrotron x-ray diffraction experiments revealed that the ambient-pressure hexagonal crystal structure is retained until at least 130 GPa. Furthermore, apart from the influence of pressure on the conducting behavior of Li_5MoH_{11}, the effect of annealing time on the conducting and superconducting behaviors at room temperature and high pressure were also observed. We hypothesized that this time-dependent behavior is due to the restoration of the MoH_9 cage structure after distortion or rotation caused by pressurization. These findings provide insight on the conducting and superconducting behaviors of ternary metal hydrides that, until recently, have been mostly studied by theoretical methods.

DOI: 10.1103/PhysRevB.99.024508

I. INTRODUCTION

As the first element of the periodic table, hydrogen is predicted to be metallic and, even possibly, a high-temperature superconductor under high pressure [1,2]. Quantum mechanics calculations suggest that molecular hydrogen can form a metallic state and show superconductivity at a transition temperature (T_c) of 242 K and pressure of 450 GPa [3]. When molecular hydrogen transforms to atomic hydrogen at 500 GPa, the T_c would be higher than room temperature, specifically 356 K [4,5]. These attractive theoretical predictions provided an impetus for scientists to experimentally explore the superconductivity of hydrogen under high pressure. However, the observation of the metallization of pure hydrogen under high pressure has remained elusive despite many high-pressure experiments above 300 GPa [6–9]. Because of the inaccessibility of high pressure for hydrogen metallization at typical experimental conditions, ideas on metallic and superconducting hydrogen were extended to hydrides. On the basis of Ashcroft's suggestion, the metallization of hydrides can be achieved by current experimental techniques owing to chemical "pre-compression" from relatively heavier elements [10]. Subsequently, numerous hydrogen-rich hydrides have been predicted to show metallic phases and even superconductivity under high pressure [11–20]. Several theoretical studies have indicated that the high-pressure phases of silane exhibit a metallic state and superconducting behavior at T_c values from 16 to 55 K under high pressure [11–13]. Silane later became the hydride to experimentally exhibit superconducting behavior at a T_c of 17 K at 96 and 120 GPa [21], despite intensive debates [22–24]. Another hydride that showed superconducting behavior was sulfur hydride, which, surprisingly, had a T_c of 203 K at 150 GPa [25]. Additionally, this experimental T_c value, as well as the body-centered-cubic structure of the superconducting phase, matched the theoretical calculations well [16,26]. This discovery has generated significant interest in exploring other hydrides that could be a 3 kind of high-T_c superconductor. The hydrogen-rich metal hydrides, CaH_6 [17], YH_6 [18], MgH_6 [19], YH_{10}, and LaH_{10} [20], which have a sodalite-like cage structure, have become increasingly attractive owing to the potentially high T_c (>200 K or even room temperature) under high pressure. Recently, the successful synthesis of LaH_{10+x} from La and H_2 at about 170 GPa and 1000 K was reported [27]. However, experiments are difficult to implement because of slashing experimental conditions of 170 GPa and 1000 K.

Ternary hydrides can be regarded as doped binary hydrides; thus, they are also believed to show metallization (at pressures lower than that of pure hydrogen) and possibly, high-temperature superconductivity [28]. Following this idea, theoretical models of ternary metal hydrides were constructed by introducing a metal into a hydride, and systems such as $MgCH_4$ [28], $MgSiH_6$ [29], $MgGeH_6$ [30], and Fe_2SH_3 [31] showed superconductivity under high pressure. Synthesis of

*Author to whom correspondence should be addressed: meng@hpr.stec.es.osaka-u.ac.jp

these hydrides is underway. Transition metal hydrides show hydrogen-rich coordination with cage structure because of covalent bonding between transition metal and hydrogen atoms [32]. In these hydrides, such as $MgFeH_6$, Mg_3CrH_8, $BaReH_9$, and Li_5MoH_{11}, the transition metal can be surrounded by more than six hydrogen atoms [33–35]. Moreover, compared with binary metal hydrides, which are synthesized at high pressure, ternary transition metal hydrides usually require mild pressures (below 10 GPa) for synthesis and can be recovered under ambient pressure. Electrical conductivity experiments showed that the ternary transition metal hydride, $BaReH_9$, is a superconductor at pressures above 100 GPa with a maximum T_c of 7 K [36].

This study focused on the transition metal hydride, Li_5MoH_{11}, which has a hexagonal crystal structure, wherein Li^+, H^-, and the ninefold-hydrogen-coordinated $[MoH_9]^{3-}$ form ionic bonds. Density of states calculations indicated that the hydrogen 1*s* orbital is strongly hybridized with Mo *spd* states to form a σ-bond and reach the Fermi level [35]. The high hydrogen number can promote the hybridization of hydrogen and the transition metal and furthermore, a high T_c. Moreover, calculations of competing phase structures under compression predicted that a phase transition from MoH_9 (with ninefold hydrogen coordination) to MoH_{11} (with 11-fold hydrogen coordination) occurs at around 94 GPa, thereby changing the transition metal hydride from an insulator to a metal. Thus, the conducting and superconducting behaviors of Li_5MoH_{11} become intriguing under high pressure. Li_5MoH_{11} is expected to show metallization and possibly, high T_c superconductivity, upon application of pressure. These two phenomena were investigated under high pressure by electrical resistance measurements. In addition, synchrotron powder x-ray diffraction (XRD) was carried out to understand the pressure dependence of phase transition.

II. EXPERIMENTAL DETAILS

Li_5MoH_{11} was synthesized using the high-pressure, high-temperature method described in Ref. [35]. A diamond anvil cell was used for pressurization. The culet size of the beveled diamond was 100–300 μm and the angle was 8°. The gasket was a 250-μm rhenium plate preindented to 25 μm and drilled with a 130-μm-diameter hole filled with a mixture of cubic boron nitride (*c*-BN) and epoxy, which was pressured to a thickness of 25 μm. A sample chamber with a diameter of 32 μm was drilled into the *c*-BN layer. The resistance was measured with electrical probes made of Pt foil and an Au film using a four-probe method [37]. The outer part of the electrical probe is a Pt foil set on the surface of *c*-BN, while the inner part is an Au film deposited on the surface of the top diamond. The Pt foil and Au film were connected during pressurization. Sample loading was performed in a glovebox under argon atmosphere to prevent decomposition or any other chemical reaction. To ensure that all resistance signals come from the sample itself, no pressure medium was used in this experiment. The pressure dependence of the resistance of the sample was measured in the AC four-terminal measurement mode. The pressure was gauged at room temperature using the diamond Raman method described by Akahama [38]. The sample was cooled using liquid helium and a ^{3}He/^{4}He dilution refrigerator. The synchrotron powder XRD experiment was performed at Beamline BL10XU of the SPring-8 synchrotron radiation facility (Hyogo, Japan). The beams were monochromatized to a wavelength of 0.41499 Å and collimated to a diameter of 10 μm. The XRD signals were collected by the imaging plate x-ray area detector system.

III. RESULTS AND DISCUSSION

Li_5MoH_{11} is an insulator at ambient pressure. During pressurization at room temperature, the resistance drops by two orders of magnitude until the pressure reaches 100 GPa, as shown in Fig. 1(a). The resistance stabilizes above 100 GPa, at which the resistivity is around 0.001 Ω cm. This corresponds to a conductivity of 1000 S cm^{-1}, which is close to the minimum conductivity of a metal [39,40]. Thus, Li_5MoH_{11} transforms from an insulator to a poor metal at room temperature and pressures above 100 GPa. Intriguingly, a rapid decrease in the room-temperature resistance is detected between 90 and 100 GPa. At 100 GPa and room temperature, the resistance declines continuously; it decreases from 48 (point A) to 17 Ω (point B) after 13 days and stabilizes at 10 Ω (point C) after another 22 days, as shown in Fig. 1(b). The sample notably presents insulating behavior, which is suppressed with increasing annealing time, as indicated by the increase in the slope of the resistance-temperature (*R-T*) curve (*dR/dT*). Thus, the conducting behavior of Li_5MoH_{11} is affected not only by pressure but also the duration of annealing. This time dependence of the conducting behavior is also reported for $BaReH_9$, whose superconductivity emerges within a time period of 77 days at 139 GPa [36].

With a further pressure increase to 130 GPa, the resistance drops abruptly near 3 K and levels at 1 K in the *R-T* curve, which represents the superconducting transition. This superconducting behavior can be retained with a further increase in pressure up to 170 GPa, as shown in Fig. 1(c). To confirm superconductivity, an incremental magnetic field was applied to the sample at 140 GPa. Superconductivity is suppressed by the magnetic field, and no resistance drop occurs at a magnetic field of 4 T when the sample is cooled down to 1 K, as shown in Fig. 1(d). To further understand this behavior, the relationship between the upper critical field H_{c2} and onset T_c is plotted in the inset of Fig. 1(d). The dashed line represents the slope of the linear fitting of $H_{c2}[(dH_{c2}/dT)_{T=T_c}]$. The H_{c2} at 0 K can be estimated using the Werthamer-Helfand-Hohenberg formula, $H_{c2}(0) = -0.693T_c(dH_{c2}/dT)_{T=T_c}$ [41]. The calculated H_{c2} at 0 K is 4.5 T, which is consistent with experimental data indicating that a magnetic field of 4 T can restrain superconductivity. The high H_{c2} signifies that this new superconductor is likely a type-II superconductor. T_c is defined as the deviation of the resistance curve from the linear temperature dependence, as described in Fig. 1(d). Zero resistance cannot be obtained mainly because of the deformation resistance that includes the nonsuperconducting part of the sample in series with the measuring path. The observed drop in resistance cannot be attributed to the Re gasket because the T_c of Re is 1.7 K at room temperature, reaches its peak (3.5 K) at 5 GPa, and is lower than 2 K when the pressure is higher than 60 GPa [42,43]. One of the starting materials of Li_5MoH_{11},

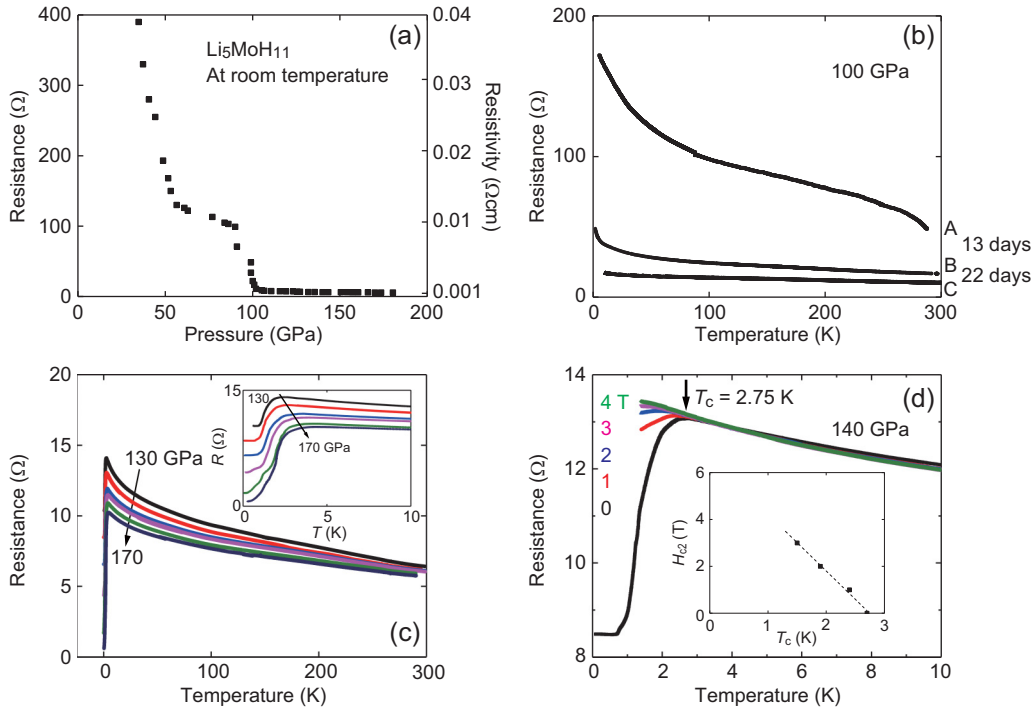

FIG. 1. (a) Pressure dependence of electrical resistance of Li_5MoH_{11} at room temperature. Temperature dependence of resistance at various pressures: (b) 100 GPa at various annealing times, (c) 130–170 GPa at 0–300 K (inset: 0–10 K), and (d) 140 GPa at various magnetic fields. The inset shows upper critical field H_{c2} at various transition temperatures T_c, which are determined from the onset of resistance drop. The dashed line is the linear fitting with slope $(dH_{c2}/dT)_{T=T_c}$.

Mo, has a T_c of around 1 K [44]; thus, the possibility that Re and Mo are in the superconducting phase can be excluded.

At ambient pressure, the crystal structure of Li_5MoH_{11} is hexagonal with space group $P6_3cm$ (No. 185). To confirm the pure phase, Rietveld analysis of the powder XRD pattern measured at ambient pressure was performed using the RIETAIN-2000 program [45,46]. Figure 2(a) shows that refinement parameters R_{wp} and R_p are 3.46% and 2.03%, respectively, which agree with previous results well [35]. High-pressure synchrotron powder XRD of Li_5MoH_{11} was conducted at room temperature to comprehensively understand the structural phase transition. A pressure medium was not used, and the maximum pressure was 130 GPa. Figure 2(b) shows the XRD patterns from 6 to 130 GPa. The results indicate that the ambient-pressure hexagonal structure of Li_5MoH_{11} is maintained up to 130 GPa. In powder XRD measurements, the determination of the crystal structure is based on the electron density of the atoms. The position of hydrogen atoms cannot be determined owing to its low electron density; therefore, it is not reflected on the powder XRD data. The hexagonal structure defined by the Mo lattice is maintained up to 130 GPa. The sample was annealed at room temperature and 100 GPa for 37 days to monitor the time-dependent behavior. The hexagonal structure is held and no new phase appeared after annealing, indicating that the time-dependent behavior is not related to structural change. Furthermore, the emergence of superconducting behavior cannot be ascribed to the transition of the hexagonal structure. These results demonstrate that phase transition from $P6_3cm$ to Cc at 5 GPa and Cc to Pc at 94 GPa do not occur as predicted by theory [35]. Similar to Li_5MoH_{11}, $BaReH_9$ shows no structural phase transition up to 110 GPa [36]. The continuous shift of the peaks to higher wavenumbers imply the shrinkage of the lattice parameters. The plots of lattice parameters a and c as a function of pressure shows that lattice parameters decrease gradually with increasing pressure up to 130 GPa [Fig. 2(c)]. Figure 2(d) shows the pressure dependence of the unit cell volume, which is compressed by 54% at a pressure of 130 GPa. The solid curve represents the best-fit curve to the third-order Birch-Murnaghan equation of state [47], which yields a bulk modulus B_0 of 51.6 ($\pm$ 2.2) GPa and its first pressure derivative B_0' of 4.65 ($\pm$ 0.17).

In this study, electrical resistance measurements were carried out to investigate the metallization and superconductivity of Li_5MoH_{11} under high pressure. The phase diagram of Li_5MoH_{11} based on two independent runs is summarized in Fig. 3. Overall, Li_5MoH_{11} transforms from an insulator to a poor metal at around 100 GPa. Superconducting behavior emerges after metallization. Metallization and superconductivity are realized when Li_5MoH_{11} has a hexagonal structure because, as demonstrated by synchrotron powder XRD, this structure is maintained up to 130 GPa. Li_5MoH_{11} shows time-dependent behavior under high pressure, which implies that apart from the influence of pressure and temperature on electrical resistance, the effect of annealing time on resistance and conducting behavior can also be observed. $BaReH_9$ also exhibited time-dependent behavior, possibly owing to the distortion of the ReH_9 unit, and its superconductivity emerged with an extended time of 77 days [36]. Because the bonding state in MoH_9 is similar to that in ReH_9, we hypothesize that the time-dependent behavior of Li_5MoH_{11} also arises from the recovery of hydrogen cages around the Mo atoms after

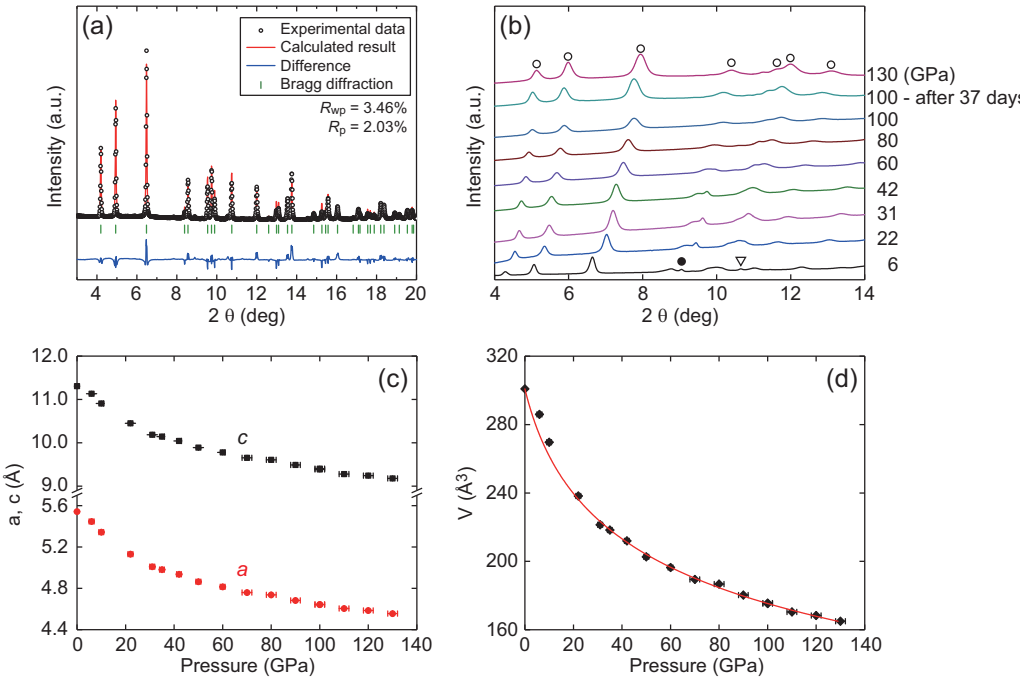

FIG. 2. (a) Powder XRD pattern of Li_5MoH_{11} at ambient pressure and Rietveld refinement parameters R_{wp} and R_p. (b) Powder XRD pattern at various pressures up to 130 GPa and room temperature. Open circles indicate the reflection from Li_5MoH_{11}; closed circle, Li_2O; and open triangle, tungsten (needle used to load sample into diamond anvil cell). (c) Pressure dependence of lattice parameters a and c. (d) Unit cell volume V as a function of pressure. The solid curve is the best-fit curve to the third-order Birch-Murnaghan equation of state. Data fitting yields a bulk modulus B_0 of 51.6 (±2.2) GPa and its first pressure derivative B_0' of 4.65 (±0.17).

distortion or rotation due to pressurization. It was concluded from the XRD results that the time-dependent behavior is not induced by the transition of the hexagonal structure, although the position of hydrogen atoms cannot be determined. In the Li_5MoH_{11} structure, Mo and H atoms hybridize and form a MoH_9 unit with ninefold hydrogen coordination. MoH_9 prisms are distorted by high pressure and then restored after a time lapse to a more stable state. The recovery time can last 48 days at 100 GPa for Li_5MoH_{11} and 77 days at 139 GPa for $BaReH_9$. The pressure-time path plays an important role in the conducting behavior of Li_5MoH_{11}. Additionally, based on the calculated electronic structure, the physical properties of Li_5MoH_{11} are also dominated by the MoH_9 unit [35]. It can be seen from Fig. 3 that the T_c from the two independent runs do not match well. We hypothesize that this is due to the different room-temperature annealing time under high pressure. At 100 GPa, the annealing time was 48 days in the first run and 18 days in the second run, and this would lead to a discrepancy in the recovery of the hydrogen cage after distortion or rotation.

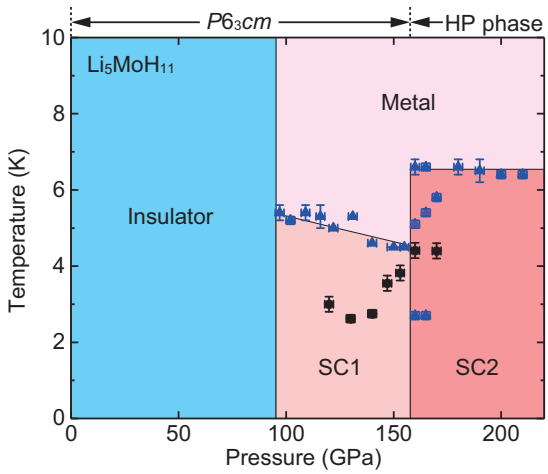

FIG. 3. Phase diagram of Li_5MoH_{11} as a function of pressure. The black squares and blue triangles represent data from run 1 and run 2, respectively. The annealing time was 48 days for run 1 and 18 days for run 2. HP indicates high-pressure, and SC1 and SC2 indicate superconducting phases. The different values of T_c at 160 and 165 GPa in SC2 indicate the coexistence of high-pressure superconducting phases.

Two different superconducting phases (SC1 and SC2) are defined in the phase diagram because evidence of a possible phase transition is observed at 160 GPa in the second run (Fig. 3). It is remarkable that there are three points of inflection at 160 GPa but only one at 150 GPa in the *R-T* curve, as shown in Fig. 4(a). Moreover, these inflections are suppressed by applying magnetic fields of up to 6 T. Figure 4(b) shows the temperature dependence of H_{c2} at 150 and 160 GPa. The estimated value of $H_{c2}(0)$ at 160 GPa is 13.7 T, which is much higher than that at 150 GPa (5.3 T). This may be explained by the coexistence of three high-pressure phases. For $BaReH_9$, two inflection points with similar behavior are recognized at 91 GPa [36]. In addition, Ying *et al.* reported a similar discrepancy in H_{c2} at different pressures due to phase transition, as proven by Raman measurement [48]. Thus, these results

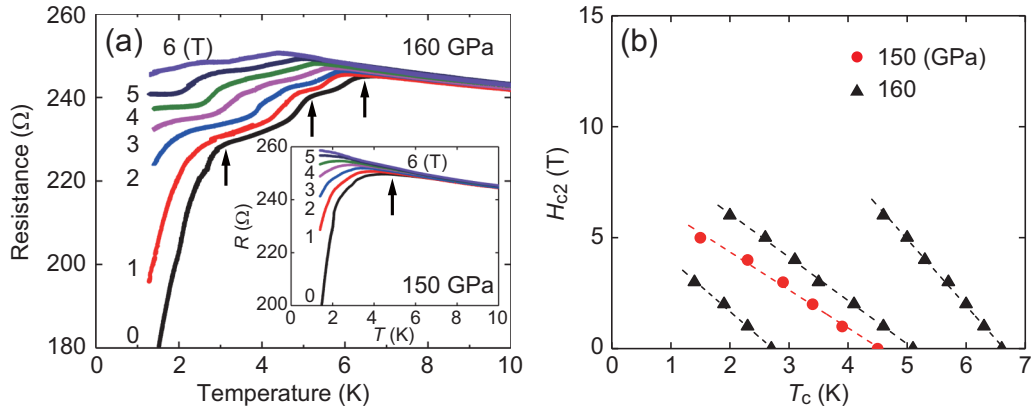

FIG. 4. (a) Resistance as a function of temperature at various magnetic fields and 160 GPa (inset: 150 GPa). (b) Transition temperature T_c dependence of upper critical field H_{c2} at 150 and 160 GPa. These three curves at 160 GPa correspond to three points of inflection.

may indicate a possible phase transition at 160 GPa. Several phases coexist between 160 and 170 GPa and transform to a single phase above 170 GPa. A synchrotron powder XRD measurement at pressures up to 170 GPa is necessary to verify this hypothesized phase transition.

Both Li_5MoH_{11} and $BaReH_9$ exhibit time-dependent behavior. Furthermore, several possible superconducting phases appear for both transition metal hydrides. The T_c and pressure region of their superconducting phases are also quite similar. These similarities may be attributed to their hexagonal crystal structure, which includes the MH_9 (M: Re, Mo) unit hybridized by the transition metal and hydrogen atoms. The conducting and superconducting behaviors are affected by the MH_9 cage structure. Based on the phase diagrams of $BaReH_9$ and Li_5MoH_{11}, the distortion or rotation of the cage structure with time-dependent effects may change T_c. On the other hand, the $BaReH_9$ phase diagram notably shows a dome-shaped superconducting phase between 80 and 150 GPa, whereas the T_c of Li_5MoH_{11} begins at 100 GPa, remains at 6.5 K from 160 to 210 GPa, and decreases to 4.5 K at 155 GPa. The superconducting phase of Li_5MoH_{11} is obtained above 200 GPa. Moreover, unlike the emergence of superconductivity in $BaReH_9$, there is no evident change in resistance and accelerated superconducting behavior in Li_5MoH_{11} upon laser irradiation.

IV. CONCLUSIONS

In summary, electrical resistance and synchrotron powder XRD measurements of the hydrogen-rich metal hydride, Li_5MoH_{11}, were carried out at pressures of up to 210 GPa. Metallization of Li_5MoH_{11} was realized at around 100 GPa and room temperature. Superconductivity emerged from around 100 to 210 GPa with a maximum T_c of 6.5 K. The XRD data indicated that the hexagonal structure is maintained at pressures up to 130 GPa. The room-temperature annealing time had an effect on T_c and its corresponding pressure. These results provide more information about the behavior of the superconducting family of hydrogen-rich ternary metal hydrides.

ACKNOWLEDGMENTS

This work was supported by Japan Society for the Promotion of Science (JSPS) KAKENHI Specially Promoted Research Grant No. 26000006; JSPS KAKENHI Grant No. 16H06119; Ministry of Education, Culture, Sports, Science, and Technology (MEXT) KAKENHI JP18H05513; and the China Scholarship Council Program. The authors thank N. Warifune from Tohoku University for assistance with sample synthesis.

[1] N. W. Ashcroft, Phys. Rev. Lett. **21**, 1748 (1968).
[2] C. F. Richardson and N. W. Ashcroft, Phys. Rev. Lett. **78**, 118 (1997).
[3] P. Cudazzo, G. Profeta, A. Sanna, A. Floris, A. Continenza, S. Massidda, and E. K. U. Gross, Phys. Rev. Lett. **100**, 257001 (2008).
[4] J. M. McMahon and D. M. Ceperley, Phys. Rev. B **84**, 144515 (2011).
[5] J. M. McMahon, M. A. Morales, C. Pierleoni, and D. M. Ceperley, Rev. Mod. Phys. **84**, 1607 (2012).
[6] M. I. Eremets and I. A. Troyan, Nat. Mater. **10**, 927 (2011).
[7] R. P. Dias and I. F. Silvera, Science **355**, 715 (2017).
[8] X. D. Liu, P. D. Simpson, R. T. Howie, B. Li, and E. Gregoryanz, Science **357**, 2286 (2017).
[9] A. F. Goncharov and V. V. Struzhkin, Science **357**, 9736 (2017).
[10] N. W. Ashcroft, Phys. Rev. Lett. **92**, 187002 (2004).
[11] Y. Yao, J. S. Tse, Y. Ma, and K. Tanaka, Europhys. Lett. **78**, 37003 (2007).
[12] X. J. Chen, J. L. Wang, V. V. Struzhkin, H. K. Mao, R. J. Hemley, and H. Q. Lin, Phys. Rev. Lett. **101**, 077002 (2008).
[13] M. Martinez-Canales, A. R. Oganov, Y. Ma, Y. Yan, A. O. Lyakhov, and A. Bergara, Phys. Rev. Lett. **102**, 087005 (2009).
[14] J. S. Tse, Y. Yao, and K. Tanaka, Phys. Rev. Lett. **98**, 117004 (2007).

[15] G. Gao, A. R. Oganov, A. Bergara, M. Martinez-Canales, T. Cui, T. Iitaka, Y. Ma, and G. Zou, Phys. Rev. Lett. **101**, 107002 (2008).
[16] D. Duan, Y. Liu, F. Tian, D. Li, X. Huang, Z. Zhao, H. Yu, B. Liu, W. Tian, and T. Cui, Sci. Rep. **4**, 6968 (2014).
[17] H. Wang, J. S. Tse, K. Tanaka, T. Iitaka, and Y. Ma, Proc. Natl. Acad. Sci. USA **109**, 6463 (2012).
[18] Y. Li, J. Hao, H. Liu, J. S. Tse, Y. Wang, and Y. Ma, Sci. Rep. **5**, 9948 (2015).
[19] F. Peng, Y. Sun, C. J. Pickard, R. J. Needs, Q. Wu, and Y. Ma, Phys. Rev. Lett. **119**, 107001 (2017).
[20] H. Liu, I. I. Naumov, R. Hoffmann, N. W. Ashcroft, and R. J. Hemley, Proc. Natl. Acad. Sci. USA **114**, 6990 (2017).
[21] M. I. Eremets, I. A. Trojan, S. A. Medvedev, J. S. Tse, and Y. Yao, Science **319**, 1506 (2008).
[22] O. Degtyareva, J. E. Proctor, C. L. Guillaume, E. Gregoryanz, and M. Hanfland, Solid State Commun. **149**, 1583 (2009).
[23] T. A. Strobel, A. F. Goncharov, C. T. Seagle, Z. Liu, M. Somayazulu, V. V. Struzhkin, and R. J. Hemley, Phys. Rev. B **83**, 144102 (2011).
[24] M. Hanfland, J. E. Proctor, C. L. Guillaume, O. Degtyareva, and E. Gregoryanz, Phys. Rev. Lett. **106**, 095503 (2011).
[25] A. P. Drozdov, M. I. Eremets, I. A. Troyan, V. Ksenofontov, and S. I. Shylin, Nature (London) **525**, 73 (2015).
[26] M. Einaga, M. Sakata, T. Ishikawa, K. Shimizu, M. I. Eremets, A. P. Drozdov, I. Troyan, N. Hirao, and Y. Ohishi, Nat. Phys. **12**, 835 (2016).
[27] Z. M. Geballe, H. Liu, A. K. Mishra, M. Ahart, M. Somayazulu, Y. Meng, M. Baldini, and R. J. Hemley, Angew. Chem., Int. Ed. **57**, 688 (2018).
[28] F. Tian, D. Li, D. Duan, X. Sha, Y. Liu, T. Yang, B. Liu, and T. Cui, Mater. Res. Express **2**, 046001 (2015).
[29] Y. Ma, D. Duan, Z. Shao, H. Yu, H. Liu, F. Tian, X. Huang, D. Li, B. Liu, and T. Cui, Phys. Rev. B **96**, 144518 (2017).
[30] Y. Ma, D. Duan, Z. Shao, D. Li, L. Wang, H. Yu, F. Tian, H. Xie, B. Liu, and T. Cui, Phys. Chem. Chem. Phys. **19**, 27406 (2017).
[31] S. Zhang, L. Zhu, H. Liu, and G. Yang, Inorg. Chem. **55**, 11434 (2016).
[32] S. Takagi and S. Orimo, Scr. Mater. **109**, 1 (2015).
[33] S. Takagi, Y. Iijima, T. Sato, H. Saitoh, K. Ikeda, T. Otomo, K. Miwa, T. Ikeshoji, K. Aoki, and S. Orimo, Angew. Chem., Int. Ed. **54**, 5650 (2015).
[34] N. T. Stetson, K. Yvon, and P. Fischer, Inorg. Chem. **33**, 4598 (1994).
[35] S. Takagi, Y. Iijima, T. Sato, H. Saitoh, K. Ikeda, T. Otomo, K. Miwa, T. Ikeshoji, and S. Orimo, Sci. Rep. **7**, 44253 (2017).
[36] T. Muramatsu, W. K. Wanene, M. Somayazulu, E. Vinitsky, D. Chandra, T. A. Strobel, V. V. Struzhkin, and R. J. Hemley, J. Phys. Chem. C **119**, 18007 (2015).
[37] K. Shimizu, J. Phys. Condens. Matter. **19**, 125207 (2007).
[38] Y. Akahama and H. Kawamura, J. Appl. Phys. **100**, 043516 (2006).
[39] M. I. Eremets, V. V. Struzhkin, H. K. Mao, and R. Hemley, Science **293**, 272 (2001).
[40] N. F. Mott, *Metal-Insulator Transition*, 2nd ed. (Taylor & Francis, London, 1990).
[41] N. R. Werthamer, E. Helfand, and P. C. Hohenberg, Phys. Rev. **147**, 295 (1966).
[42] C. W. Chu, T. F. Smith, and W. E. Gardner, Phys. Rev. Lett. **20**, 198 (1968).
[43] K. Takahama, T. Matsuoka, and K. Shimizu (unpublished).
[44] J. J. Hamlin, Physica C **514**, 59 (2015).
[45] H. M. Rietveld, J. Appl. Cryst. **2**, 65 (1969).
[46] F. Izumi and T. Ikeda, Mater. Sci. Forum **321–324**, 198 (2000).
[47] F. Birch, Phys. Rev. **71**, 809 (1947).
[48] J.-J. Ying, V. V. Struzhkin, Z.-Y. Cao, A. F. Goncharov, H.-K. Mao, F. Chen, X.-H. Chen, A. G. Gavriliuk, and X.-J. Chen, Phys. Rev. B **93**, 100504 (2016).